

# An Analysis on Singular Fields around an Interface Edge of Ceramic/Metal Joints Using Moiré Interferometry Technique\*

Samadder LITON KUMAR\*\*, Yoshio ARAI\*\*\* and Eiichiro TSUCHIDA\*\*\*

Characteristics of singular fields around an interface edge between ceramic and soft metallic interlayer were investigated experimentally and theoretically. Displacement fields around the interface edge were measured by means of high-sensitivity moiré interferometry. The measured singular fields around the elastic/elastic-plastic interface edge were compared with theoretical results (an elastic/linear hardening materials interface edge prediction and an elastic/power-law hardening materials interface edge prediction). Intensification of stress concentration around the interface edge due to the plastic deformation of the interlayer was clearly observed experimentally and illustrated based on the analysis. A controlling factor for the evolution of singular fields around the elastic/elastic-plastic materials interface edge was proposed and its validity was examined.

**Key Words:** Interface, Interface Mechanics, Elastic Plastic, Stress Analysis, Singular Field, Stress Concentration

## 1. Introduction

For strength evaluations of ceramic/metal joints it is important to clarify characteristics of stress fields around an interface edge of the joints<sup>(1)</sup>. There has been many experimental and theoretical investigations on the stress distribution of ceramic/metal joints<sup>(2)–(4)</sup>. Cao et al. examined evolutions of plastic zones in the metal side of ceramic/metal joints<sup>(5)</sup>. Post et al. measured thermal stress distributions around an interface edge of joined plates which have different thermal expansion coefficients by means of high-sensitivity moiré<sup>(6)</sup>. Analytical studies on the stress singularity around the interface edge of elastic/elastic-plastic materials joint have been conducted by many researchers. Duva, Rahman and Reedy modeled the elastic/power-law hardening plastic materials joint as a power-law hardening plastic materials on a rigid substrate<sup>(7)–(9)</sup>. They conducted the asymptotic analysis similar to the nonlinear crack problem developed by Hutchinson<sup>(10)</sup>. Xu et al. and Arai et al. independently proposed the analogue of the linear hardening materials joint and elastic materials joint<sup>(11),(12)</sup>. The stress fields

around the interface edge can be expressed by  $r^{\lambda-1}$  for the power-law hardening/rigid materials joints and the power-law hardening materials joints which have the same power index,  $n$ , where  $r$  is the distance from the interface edge and  $\lambda$  is the eigen value. Linear hardening materials joints can be a special case when the power  $n = 1$  in the latter joints. In many cases ceramic/metal joints which are joined at some elevated temperature have an interlayer between the ceramics and the metal to reduce the thermal residual stresses. When a power-law hardening material like copper is used as the interlayer, the material pair between the ceramics and the interlayer results in elastic and power-law hardening materials. The continuity condition of displacement and stress components at the interface conflicts the existence of a separable form singular solution like  $u_i \propto r^\lambda f_i(\theta)$  for the material pair where  $u_i$  is the displacement component and  $f_i(\theta)$  is the angular function. Applicability of the power-law/rigid materials joint model to ceramic/metal joints in regard to the interface edge problem should be examined by experimental facts. However the experimental approaches to the characteristics of stress singularity in ceramic/metal joints especially focusing on the yielding scale of soft metallic interlayers and its effect on the stress concentration in the ceramic side have not been presented yet.

In this study characteristics of singular fields around an interface edge between ceramic and soft metallic interlayer were investigated experimentally and theoretically.

\* Received 21st May, 2005 (No. 05-4103)

\*\* Graduate Student, Saitama University, 255 Shimo-Ohkubo, Sakura-ku, Saitama 338-8570, Japan

\*\*\* Department of Mechanical Engineering, Saitama University, 255 Shimo-Ohkubo, Sakura-ku, Saitama 338-8570, Japan. E-mail: yarai@mech.saitama-u.ac.jp

Displacement fields around the interface edge were measured by means of high-sensitivity moiré interferometry. The measured singular fields around the elastic/elastic-plastic interface edge were compared with theoretical results (an elastic/linear hardening materials interface edge prediction and an elastic/power-law hardening materials interface edge prediction). Intensification of stress concentration around the interface edge due to the plastic deformation of the interlayer was clearly observed experimentally and illustrated based on the analysis. A controlling factor for the evolution of singular fields around the elastic/elastic-plastic materials interface edge was proposed and its validity was examined.

## 2. Experimental Procedures

Ceramic ( $\text{Si}_3\text{N}_4$ ), copper (Cu) and stainless steel (JIS-SUS304) were joined by the activation metal vacuum brazing method. Interlayer (Cu) of 0.4 mm thickness was used for the purpose of reducing the thermal residual stresses of the ceramic/metal joint. Material properties and joining conditions are shown in Tables 1 and 2 respectively. Figure 1 (a) shows the configuration of the specimen. Preceding the adhesion of a grating layer on the specimen surface, specimen was polished using diamond particles (1  $\mu\text{m}$  diameter). The free edge of the joint materials observed by SEM is shown in Fig. 1 (b). The shape of the edge between the free surface and the interface is sharp enough to treat as the joint of apexes with right angle ( $90^\circ$ ) within 10  $\mu\text{m}$  length scale or smaller.

Laser moiré interferometry consists of He-Ne laser (wave length 663 nm) and gratings (2 dimensional, 1200 lines/mm). A cross-line diffraction grating was formed by a replication process with PC-10C (Measurement Group Inc.) as adhesive on the specimen surface under 5 N compressional load at room temperature. The thickness of gratings was about 5  $\mu\text{m}$ . Figure 2 shows a schematic description of moiré interferometry. While four point bending load was applied on the specimen (the inner span 10 mm, the outer span 30 mm) the moiré fringe at mid region of the inner span was measured. The measured plane was in the tensile side. The strain gauge was

Table 1 Material properties

	$\text{Si}_3\text{N}_4$	Cu	SUS304
E(GPa)	304	108	196
$\nu$	0.27	0.33	0.30
$\alpha (\times 10^{-6}/^\circ\text{C})$	3.0	17.7	15.0

Table 2 Condition of joining

Brazing filler	: Ti-Ag-Cu
Temperature	: 1073~1123K
Atmosphere	: Vacuum. $1.3 \times 10^{-3}$ Pa
Interlayer	: Cu (thickness 0.4mm)

also attached on  $\text{Si}_3\text{N}_4$  side at about 3 mm apart from the  $\text{Si}_3\text{N}_4/\text{Cu}$  interface, on reverse side of the measured surface by moiré.

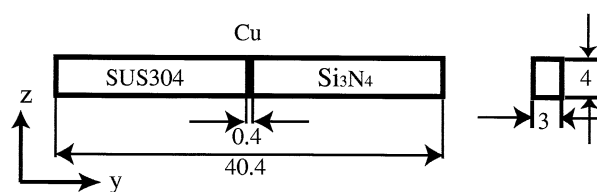
The carrier fringe and fringe shifting method was used to improve the spacial resolution<sup>(13)</sup>. In undeformed and deformed condition moiré fringes were measured. The apparent displacement,  $u_i^j(i_N)$ , can be measured from the fringe order,  $N$ ,

$$u_i^j(i_N) = \frac{N}{f}, \quad (1)$$

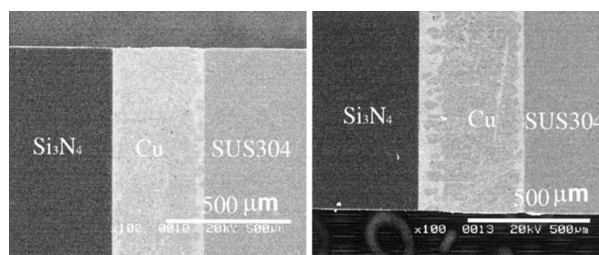
where  $u_i^j(i_N)$  is the displacement in  $i$  direction,  $i = y$  or  $z$ ,  $i_N$  is the coordinate  $i$  of the  $N$ th fringe,  $f = 2400$  [1/mm],  $j = s$  or  $c$ ,  $u_i^s(i_N)$  is the apparent displacement in deformed state calculated from the  $N$ th fringe at  $i_N$ ,  $u_i^c(i_N)$  is the apparent displacement in undeformed state calculated from the linear approximation of the carrier fringes at  $i_N$ . The true displacement components  $u_i(i_N)$  was evaluated as the change due to the deformation,

$$u_i(i_N) = u_i^s(i_N) - u_i^c(i_N). \quad (2)$$

The ideal resolution of the displacement measurement can be estimated by following equation,



(a)



(b)

Fig. 1 Specimen conditions. (a) Specimen configurations (unit: mm) (b) Edge geometry

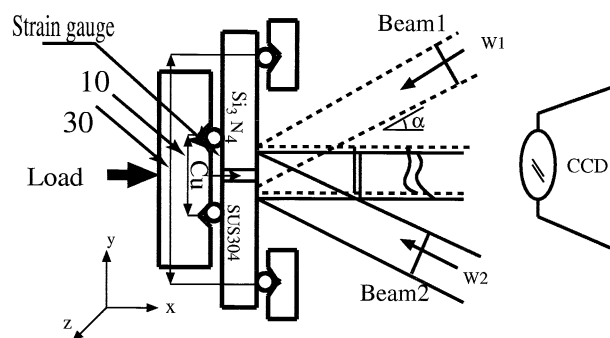


Fig. 2 Measurement system (unit: mm)

$$\Delta u_y = \pm \frac{\Delta y}{2fb}, \tag{3}$$

where  $\Delta y$  is the resolution of the coordinate,  $b$  is the interval of the carrier fringe in pixel of a digital image data. In this study  $b = 11$  [pixel],  $\Delta y = 0.00255$  mm. These values give  $\Delta u_y = \pm 4.8 \times 10^{-5}$  mm. The estimation of the coordinate of interface is an important point in the examination of singularity. In this study the coordinate of interface at the measured line (mid point of the specimen width) was estimated by interpolating between two coordinates of the exposed interface which were adjacent to the diffraction grating.

### 3. Analytical Method

Consider a joint plate shown in Fig. 3 which is subjected to bending stress at  $y = L$  with the maximum bending stress  $\sigma_y = p_0$  ( $\sigma_y = \frac{p_0}{W}(W - x)$ ,  $\tau_{yx} = 0$  at  $y = L$ ,  $u_y = 0$ ,  $\tau_{yx} = 0$  at  $y = -L$ ). The near edge stress fields for the joint plate in elastic state can be expressed as follows<sup>(3),(4),(12)</sup>,

$$u_i = p_0 k \left(\frac{r}{W}\right)^\lambda \bar{u}_i(\theta; \lambda), \tag{4}$$

$$\sigma_{ij} = p_0 k \left(\frac{r}{W}\right)^{\lambda-1} F_{ij}(\theta; \lambda), \tag{5}$$

where  $i, j$  denotes  $r$ , or  $\theta$ .  $\lambda$  is an eigen value which can be calculated as a root of the characteristic equation for the dissimilar material interface edge<sup>(3)</sup>.  $W$  is a characteristic length of the joined plates in this large aspect ratio<sup>(12)</sup>,  $k$  is a stress intensity factor with  $W$ , and  $F_{ij}(\theta; \lambda)$  is determined by  $F_{\theta\theta}(\theta = 0; \lambda) = 1$ <sup>(4)</sup>,  $\bar{u}_i(\theta; \lambda)$  is an angular function for the displacement component,  $u_i$ .

Suppose a small scale yielding condition such that the stress field outside the plastic zone around the interface edge assumed to be the one described by the elastic singular field (Eq. (5)). The plastic zone size,  $r_p$ , along the

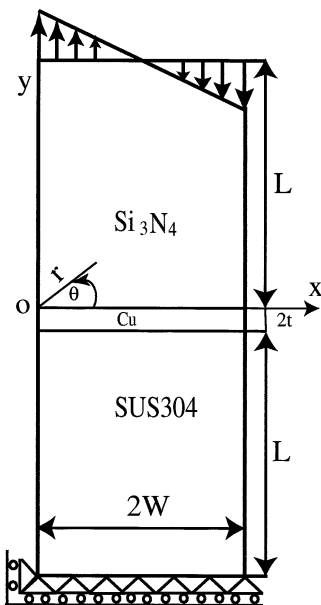


Fig. 3 Model for ceramic/metal joint subjected to bend loading

interface in the interlayer side ( $\theta = 0^-$ ) can be expressed as follows with yield strength of the interlayer,  $\sigma_{ys}$ , and the Mises yield criterion,

$$r_p = (kF_{\text{mises}})^{\frac{1}{1-\lambda}} \left(\frac{p_0}{\sigma_{ys}}\right)^{\frac{1}{1-\lambda}} W, \tag{6}$$

where  $F_{\text{mises}}$  denotes the angular function for the Mises equivalent stress which is calculated from  $F_{ij}^m(\theta = 0^-; \lambda)$ .

The order of the singularity for the linear hardening material and elastic material joint can be calculated with the elastic properties  $\nu^m$  and  $\Gamma$  replaced by the effective Poisson's ratio  $\bar{\nu}^m$  and the effective ratio of rigidity  $\bar{\Gamma}^{(12)}$ . The eigen value,  $\lambda$ , for interface edge of a joint of power-law hardening materials with different power index are considered as the one for the joint of the less hardening material on the rigid body<sup>(7)-(9)</sup>.

The stress fields were also calculated numerically by using elastoplastic finite element method. In FEM calculation, the interlayer, Cu, was assumed to be an elastic linear hardening plastic material with yield strength,  $\sigma_{ys}$ , and hardening constant,  $\omega$ <sup>(12)</sup>, or an elastic power-law hardening plastic material with hardening constant,  $\alpha$  and  $n$ . Si<sub>3</sub>N<sub>4</sub> was assumed to be elastic. Plane strain 8 nodes isoparametric elements were used. Finite element meshes were divided into 30 in the near edge area,  $0 < r/t \leq 0.1$ . The length of elements along radial direction varies as following equations,

$$l_i = \frac{l_{i-1}}{0.9}, \quad i = 1, 2, \dots, 30, \tag{7}$$

where  $l_i$  is a radial length of  $i$ -th element. The minimum length of elements,  $l_0/t$ , is  $10^{-2}$ . For circumferential direction meshes are divided into 20 by equal angle. The total number of elements is 2044 and the total number of nodes is 6307.

The stress-strain relation for the Cu tensile bar specimen which had been subjected to the same thermal condition as the joint process was experimentally measured. The specimen used for the moiré measurement had joined at the elevated temperature listed in Table 2 following cutting and machining at room temperature to the configuration shown in Fig. 1. During the joining process the interlayer, Cu, of the specimen is considered to have suffered some plastic deformation and work hardening. It is possible that the yield strength of the interlayer have changed due to the joining process. In our FEM simulation the yield strength of the interlayer, Cu, in the model was varied as listed in Table 3 to consider the effect of yield strength on the evolution of the stress singularity.

Table 3 Plastic properties of interlayer

Yield strength $\sigma_{ys}$ [MPa]	30 ~ 80
Linear hardening constant $\omega$	231
Power-law hardening index $n$	2.4
Power-law hardening constant $\alpha$	10.1

### 4. Experimental Results

Figure 4 shows an example of fringe in moiré images for displacement measurement toward  $y$  direction. The slope of the log-log plot between the displacement,  $u_y$ , and the coordinate,  $y$ , in  $\text{Si}_3\text{N}_4$  side far from the  $\text{Si}_3\text{N}_4/\text{Cu}$  interface approached to unity which is the slope in the homogeneous case as shown in Fig. 5. At the external stress of 273 MPa it was clearly seen that the slope decreased with decreasing the coordinate,  $y$ , in the  $\log u_y - \log y$  relations. The slope was in between  $\lambda = 0.6$  and  $\lambda = 0.7$  for  $y \leq 0.2$  mm. This slope is smaller than the predicted value using elastic/elastic materials interface edge theory which is calculated from the elastic modulus of  $\text{Si}_3\text{N}_4$  and Cu (“Elastic singularity,  $\lambda = 0.92$ ” designated by a solid line in Fig. 5). The slope decreased with increasing the magnitude of external stress as also shown in Fig. 5. The slope was unity at the external stress of 68 MPa while there oc-

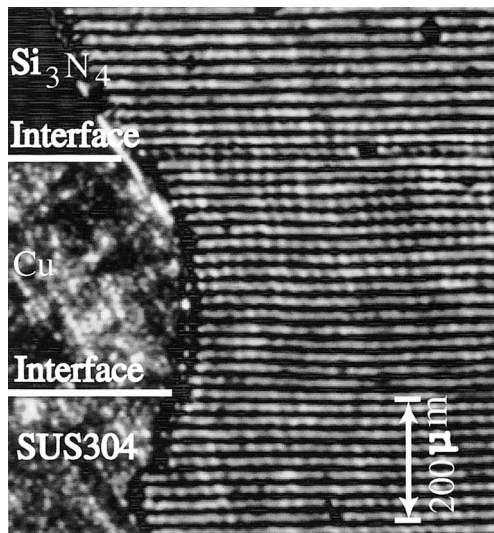


Fig. 4 A typical moiré pattern around interface ( $p_0 = 273$  MPa)

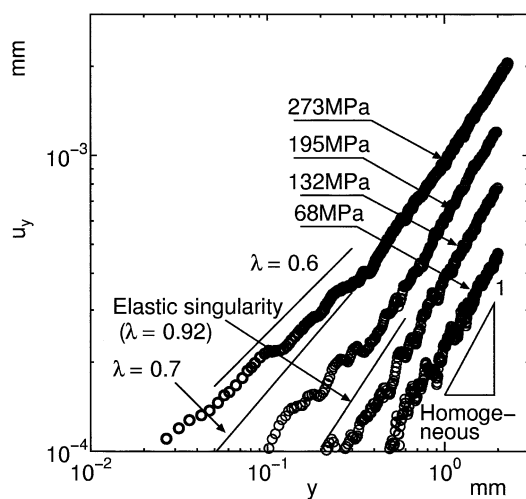


Fig. 5 Effect of external stress on log-log plot of displacement distribution

cured the  $y$  region close to the interface where the slope was between 0.6–0.7 at the external stress larger than 195 MPa.

The normal stresses to the interface,  $\sigma_y$ , coincided with the external stresses in the  $\text{Si}_3\text{N}_4$  region far from the  $\text{Si}_3\text{N}_4/\text{Cu}$  interface and the stress value increased dramatically in the small region close to the interface as shown in Fig. 6 especially at the external stress of 273 MPa. The stress value at  $y = 0.03$  mm in  $\text{Si}_3\text{N}_4$  under the external stress of 273 MPa was about four times of the stress value at the same location under the external stress of 132 MPa which is only the half value of 273 MPa as an external stress. In this study, characteristics of stress distributions were measured and examined over the finite range,  $0.03 \leq |y| \leq 0.1$  (mm). Estimation from the experimental results for the trend in  $|y| \rightarrow 0$  gives that the reason of the different stress concentration between these external stresses of 132 and 273 MPa is considered that the different scale of the plastic deformation around the interface edge gives the elastic singularity and elastic/plastic singularity for each external stress. This point will be discussed extensively later through the finite element results. The slope of the log-log plot between  $\sigma_y$  and  $y$  was between  $\lambda - 1 = -0.4 \sim -0.3$  in the region close to the interface,  $y \leq 0.2$  mm, at the external stress of 273 MPa and the slope was larger than the one for the elastic/elastic materials interface edge (Elastic singularity,  $\lambda - 1 = -0.08$ ) as shown in Fig. 6. The slope was similar to the one for the elastic/elastic materials interface edge under the external stress of 132 MPa. The slope increased with increasing the external stress. There occurred the  $y$  region close to the interface where the slope was between  $-0.3 \sim -0.4$  at the external stress larger than 195 MPa.

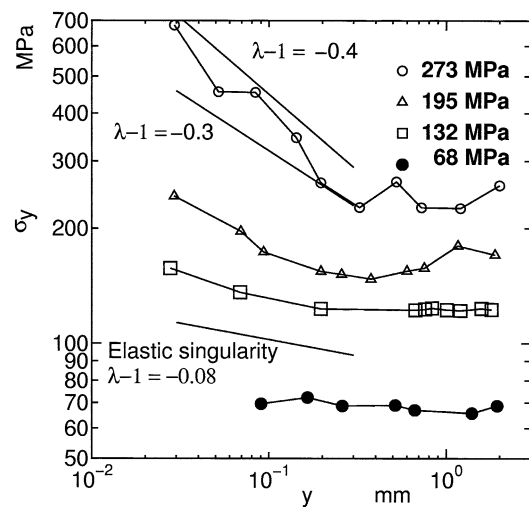


Fig. 6 Effect of external stress on log-log plot of stress distribution

5. Discussion

The slope value of the  $u_y - \log y$  relations,  $\lambda$ , was unity in the region far from the  $\text{Si}_3\text{N}_4/\text{Cu}$  interface and decreased with decreasing  $y$  at the external stress of 273 MPa as shown in Fig. 7. The  $\lambda$  approached a value between 0.6–0.7 in  $y \leq 0.1$  mm. This magnitude of  $\lambda$  was smaller than the one for the elastic/elastic materials interface edge (“Elastic singularity” in Fig. 7). The slope decreased with increasing the external stress at the same  $y$ . The linear hardening interface theory (“Linear hardening  $\omega = 231$ ” in Fig. 7) and power-law hardening/rigid interface theory (“Power-law/rigid  $n = 2.40$ ” in Fig. 7) can predict smaller  $\lambda$  compared with the elastic interface theory. It is supposed that the high stress concentration around the  $\text{Si}_3\text{N}_4/\text{Cu}$  interface edge at the large external stress is due to the difference in the effective stiffness of the plastically deforming Cu and the elastic  $\text{Si}_3\text{N}_4$ .

Dependence of normal stress distribution,  $\sigma_y$ , along  $y$  direction on the external stress predicted based on the power hardening for the interlayer, Cu, is shown in Fig. 8 with the experimental results. The yield strength of the interlayer was varied for 30, 50 and 80 MPa with the hardening constant,  $n = 2.4$ ,  $\alpha = 10.1$ . In the case of  $\sigma_{ys} = 50$  MPa the dependence of the slope in log-log plots on the external stress was predicted in good agreement with the experimental results, while in the case of  $\sigma_{ys} = 30$  MPa the slope is too large in the low external stress and in the case of  $\sigma_{ys} = 80$  MPa the slope is too small in the high external stress. From these results the evolution of the stress singularity around the interface edge of measured ceramic/metal joint can be successfully simulated by the finite element model based on the power hardening law for the interlayer with  $\sigma_{ys} = 50$  MPa and  $n = 2.4$ ,  $\alpha = 10.1$ .

The contour plots of the equivalent plastic strain  $\epsilon_p =$

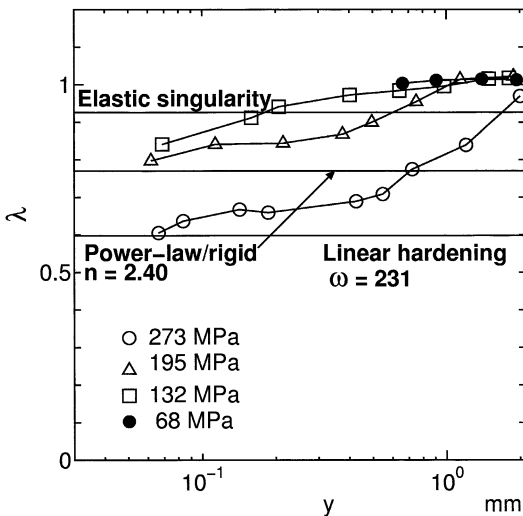


Fig. 7 Effect of external stress on slope of log-log plot of displacement distribution

0.01 at the external stresses of 132 MPa and 195 MPa are shown in Fig. 9. The yield strength for the interlayer of 50 MPa was used from the above discussion. In the small scale yielding condition shown in the case of 132 MPa in Fig. 9 in which the plastic zone size along the interface is small the singular stress field for the elastic materials interface edge described in Eq. (5) is dominant. As discussed in Eq. (6), the plastic zone size is proportional to  $(p_0/\sigma_{ys})^{1/(1-\lambda)}$  in this case. The value of  $\lambda$  is close to 1 for many elastic material joints so the value of  $1/(1-\lambda)$  becomes large (for  $\text{Si}_3\text{N}_4/\text{Cu}$  combination in elastic state,  $\lambda = 0.92$ ,  $1/(1-\lambda) = 12.5$ ). This large power for the dependence of plastic zone size on the yielding scale,  $p_0/\sigma_{ys}$ , results in an abrupt increase of the plastic zone size as the external stress increases. The external stress level which gives the abrupt increase of the plastic zone size is controlled by the yield strength of the interlayer. When given external stress is smaller than the external stress level at the abrupt increase of the plastic zone the resulted plastic zone size along the interface is small enough to neglect the effect of plastic deformation on the stress fields. In this state the elastic singularity prevails and the stress concentration at the elastic side is low. When given external stress is larger than the external stress level at the abrupt

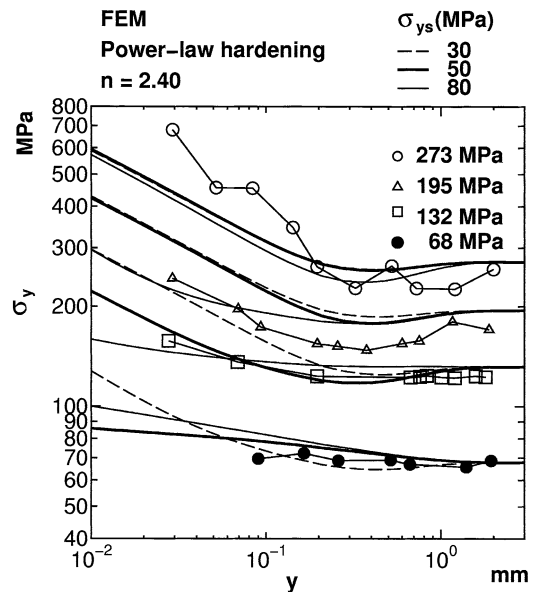


Fig. 8 Effect of yield strength of interlayer on stress distribution around interface edge

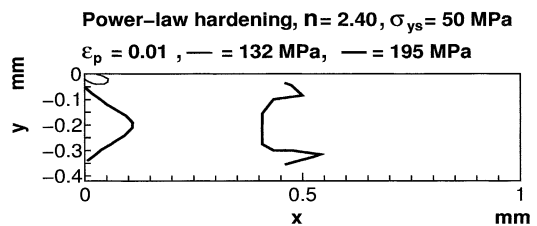


Fig. 9 Plastic zone evolution with increasing external stress

increase of the plastic zone, the plastic zone size along the interface is large and the singular stress fields for the elastic/plastic interface edge are evolved. The stress concentration at the elastic material side is large in this case. The external stress level at which the elastic/plastic effects emerged in the experimental results (the slope change in Figs. 5 and 6) is considered to be larger than 132 MPa and smaller than 195 MPa. This result coincided with the evolution of the plastic zone in the interlayer especially along the interface from the small size at the external stress of 132 MPa to the larger size at 195 MPa as illustrated in Fig. 9. From these results the yielding scale factor,  $p_0/\sigma_{ys}$ , is considered to control the evolution of the elastic/plastic singularity around the interface edge through the plastic zone size along the interface.

### 6. Conclusions

(1) The slope of the log-log plot between the displacement  $u_y$  and the coordinate  $y$  in  $\text{Si}_3\text{N}_4$  side decreased with decreasing the coordinate  $y$ . The slope was in between  $\lambda = 0.6$  and  $\lambda = 0.7$  for  $y \leq 0.2$  mm. This slope is smaller than the predicted value using elastic/elastic materials interface edge theory which is calculated from the elastic modulus of  $\text{Si}_3\text{N}_4$  and Cu.

(2) The stress value at  $y = 0.03$  mm in  $\text{Si}_3\text{N}_4$  under the external stress of 273 MPa was about four times of the stress value at the same location under the external stress of 132 MPa which is only the half value of 273 MPa as an external stress. The reason of the different stress concentration between these external stress of 132 and 273 MPa is considered that the different scale of the plastic deformation around the interface edge gives the elastic singularity and the elastic/plastic singularity for each external stress.

(3) The linear hardening interface theory and the power-law hardening/rigid interface theory can predict smaller  $\lambda$  compared with the elastic interface theory.

(4) The external stress level at which the elastic/plastic effects emerged in the experimental results coincided with the one at the evolution of the plastic zone in the interlayer especially along the interface. The yielding scale factor,  $p_0/\sigma_{ys}$ , is considered to control the evolution of the elastic/plastic singularity around the interface edge through the plastic zone size along the interface.

### References

- (1) Rühle, M., Evans, A.G., Ashby, M.F. and Hirth, J.P., Ed., Metal-Ceramic Interfaces, Acta Metall. Proc. Ser., Vol.4 (1989), Pergamon Press.
- (2) Williams, M.L., The Stress Singularities Resulting from Various Boundary Conditions in Angular Corners of Plates in Extension, Trans. ASME, J. Appl. Mech., Vol.19 (1952), pp.526–529.
- (3) Bogy, D.B., Edge-Bonded Dissimilar Orthogonal Elastic Wedges under Normal and Shear Loading, Trans. ASME, J. Appl. Mech., Vol.35 (1968), pp.460–466.
- (4) Munz, D. and Yang, Y.Y., Stress Singularities at the Interface in Bonded Dissimilar Materials under Mechanical and Thermal Loading, Trans. ASME, J. Appl. Mech., Vol.59 (1992), pp.857–861.
- (5) Cao, H.C., Thouless, M.D. and Evans, A.G., Residual Stresses and Cracking in Brittle Solids Bonded with a Thin Ductile Layer, Acta Metall. Mater., Vol.36, No.8 (1988), pp.2037–2046.
- (6) Post, D., Wood, J.D., Han, B., Parks, V.J. and Gerstle, F.P., Thermal Stresses in a Bimaterial Joint: An Experimental Analysis, Trans. ASME, J. Appl. Mech., Vol.61 (1994), pp.192–198.
- (7) Duva, J.M., The Singularity at the Apex of a Rigid Wedge after Partial Separation, Trans. ASME, J. Appl. Mech., Vol.56 (1989), pp.977–979.
- (8) Rahman, A., Singular Stress Fields at Plastically Deforming Bimaterial Interfacial Notches and Free-Edges, Ph. D. Thesis of Drexel University, (1991).
- (9) Reedy, E.D., Free-Edge Stress Intensity Factor for a Bonded Ductile Layer Subjected to Shear, Trans. ASME, J. Appl. Mech., Vol.60 (1993), pp.715–720.
- (10) Hutchinson, J.W., Singular Behaviour at the End of a Tensile Crack in a Hardening Material, J. Mech. Phys. Solids, Vol.16 (1968), pp.13–31.
- (11) Xu, J.-Q., Fu, L.-D. and Mutoh, Y., Elastic Stress Singularity at Interface Edge with Arbitrary Bonding Angle in Dissimilar Linear Hardening Materials, Trans. Jpn. Soc. Mech. Eng., (in Japanese), Vol.65, No.630, A (2000), pp.277–281.
- (12) Arai, Y., Tsuchida, E. and Sakurai, T., Study on Stress Field around Elastic/Elastic-Plastic Interface Edge, Theor. Appl. Mech., Vol.49 (2000), pp.33–39.
- (13) Post, D., Han, B. and Ifju, P., High Sensitivity Moiré, (1994), Springer-Verlag.